RSC Advances

ROYAL SOCIETY OF CHEMISTRY

www.rsc.org/advances

Water-based synthesis of zeolitic imidazolate framework-8 with high morphology level at room temperature

Meipeng Jian [a], Bao Liu [a,b], Ruiping Liu [a,*], Jiuhui Qu [a], Huanting Wang [c], Xiwang Zhang [c,*]

[a] Key Laboratory of Drinking Water Science and Technology, Research Center for Eco-Environmental Sciences, Chinese Academy of Sciences (CAS), Beijing 100085, China

[b] University of Chinese Academy of Sciences, Beijing 100049, China

[c] Department of Chemical Engineering, Monash University, Clayton, Victoria 3800, Australia

Correspondence information:

Prof. Ruiping Liu,

Tel: +86 010 6284 9160, E-mail address: liuruiping@rcees.ac.cn

Prof. Xiwang Zhang,

Tel: +61 3 9905 1867, E-mail address: xiwang.zhang@monash.edu

Abstract:

In this study, the synthesis of zeolitic imidazole framework (ZIF-8) in water was systematically studied using 6 zinc sources ($Zn(OAc)_2$, $ZnSO_4$, $Zn(NO_3)_2$, $ZnCl_2$, $ZnBr_2$, ZnI_2), respectively, under different conditions at room temperature without using any additives. It was found that $Zn(OAc)_2$ is the best precursor and the resultant ZIF-8 particles have the best quality with rhombic dodecahedron morphology. The concentration of 2-methylimidazole (Hmim), molar ratio Hmim/Zn and water content all have significant impacts on the morphology, particle size, and crystallinity of ZIF-8. Further result analysis reveals that 3 key reactions are involved in the ZIF-8 formation which needs five steps in ZIF-8 structural evolution. This study provides deep understanding of crystallization process of ZIF-8 particles in the water-based system.

Keywords: Zeolitic imidazolate framework-8; Water; Morphology; Size; Growth mechanism.

1. Introduction

Metal organic frameworks (MOFs), also known as porous coordination polymers, are a novel class of highly porous materials, which have gained considerable attention recently due to their intrinsic properties, such as high surface areas, large pore volumes, tunable pore sizes, high crystallinity and designable organic ligands.[1,2] Specifically, zeolitic imidazolate frameworks (ZIFs) are a subclass of MOFs with zeolite topologies conducted by bridging tetrahedral metal ions (e.g. Zn, Co, Cd) with imidazolate-like ligands, which possess several unique features owing to the simultaneous characteristics of both MOFs and zeolites, such as ultrahigh surface areas, unimodal micropores, abundant functionalities, exceptional chemically robustness and thermally stable stability.[3] As a result, ZIFs materials hold great promise in many practical application fields including gas storage/separation,[4] catalysis,[5,6] chemical sensing,[7,8] biomedicine[9] and water treatment.[10,11]

Among various ZIF materials, ZIF-8 is the one of the most studied ZIF materials with sodalite (SOD) topology, exhibiting a three-dimensional (3D) structure formed by zinc ions and 2-methylimidazole (Hmim) linker. Similarly, ZIF-8 has large pore cages with diameters of 11.6 Å and possesses high thermal robustness (550 ^{o}C in N_2), large surface area (BET: 1630-1700 m^2/g), and remarkable chemical resistance to various solvents including alkaline water and organic solvents.[12,13]

To date, a variety of ZIF-8 synthetic methods including hydro-/solvothermal, microwave-assisted, sonochemical and electrochemical routines have been developed to fabricate ZIF-8 at temperatures varying from room temperature up to 200 ^{o}C in

different solutions.[14] For example, Chen's group reported the synthesis of ZIF-8 crystals for the first time in methanol and aqueous ammonia as the reaction medium, respectively, in 2006.[15] In the same year, Yaghi's group synthesized ZIF-8 in N,N-dimethylformamide (DMF) at 140 ^{o}C.[12] Later, Cravillon et al. produced ZIF-8 nanocrystals using a facile routine where $Zn(NO_3)_2$ and Hmim are mixed in methanol at room temperature.[16] Inspired by these pioneering works, different novel synthesis strategies with the assistance of additives (such as triethylamine,[17] sodium formate,[18] n-butylamine[19] and polyamine[20]) in the organic-based solution system were developed to optimize preparation conditions and control over the morphology and size of ZIF-8. However, organic solvents are usually expensive and toxic. Moreover, some organic solvents like DMF are difficult to be removed from pores of ZIF-8 crystals.[21] Therefore, increasing effort has recently been devoted to developing green approaches without using any organic solvents to prepare ZIF-8. Although, several modified syntheses methods with adding modulating agents have been reported to promote the formation and tune textural property of ZIF-8 material,[17,22,23] it still remains a challenge to synthesize pure ZIF-8 crystals with highly regular particle morphology in water at room temperature without using any additives. Pan et al. first reported the successful synthesis of ZIF-8 in water at room temperature without using any additives.[24] However, excess amount of Hmim is needed in this method. Visible defects and blurred rhombic dodecahedral shape were observed on the synthesized ZIF-8 crystals when less Hmim was used.[25] In principal, the morphologies and crystallinities of ZIF-8 are controlled by some key factors including zinc source,

Hmim/Zinc ratio, water amount, etc. Unfortunately, there is still a lack of comprehensive study on the effect of these factors, which hinders the development of green synthesis of ZIFs.

Herein, we conducted a systematic study on the synthesis of ZIF-8 in water using six common zinc sources under different conditions at room temperature without using any additives. Furthermore, the crystallization kinetics of ZIF-8 has also been monitored by power X-ray diffraction (XRD) and field emission scanning electron microscopy (SEM) at different time intervals to reveal the crystal growth mechanism in water.

2. Experimental

2.1 Materials

$Zn(OAc)_2$ (≥ 99%), $ZnSO_4$ (≥ 99%), $Zn(NO_3)_2 \cdot 6H_2O$ (≥ 98%), $ZnCl_2$ (≥ 98%), $ZnBr_2$ (≥ 98%), ZnI_2 (≥ 99%) and 2-methylimidazole (Hmim, ≥ 99%) were purchased from Sigma Aldrich. All chemicals were used as received without further purification. The deionized (DI) water with a resistivity of 18.2 MΩ/cm used throughout the experiments was purified with a water ultra-purification system (Milli-Q Advantage A10, Merck Millipore, USA).

2.2 Synthesis of ZIF-8 crystals

Typically, 293 mg of $Zn(OAc)_2$ was first dissolved in 10 mL of DI water and then the solution added to another solution consisting of 1.08 g of Hmim in 20 mL of DI water without stirring at room temperature (~25 ± 2 ^oC). The final molar

composition of the synthesis solution was Zn/Hmim/water = 1/35/1280. After aging for 24 h, the precipitate was separated from the colloidal dispersion by centrifugation (7000 rpm, 5 min) and washed with DI water three times. To examine the effects of the molar ratio of Hmim/Zn on the as-synthesized products, the Hmim/Zn molar ratio was adjusted from 10 to 70 by adjusting the concentration of Hmim at a fixed Zn concentration (0.78 mmol/L). Finally, the obtained products were then dried in air for 24 h at 60 ^{o}C for subsequent characterization. Syntheses of ZIF-8 using other zinc sources, e.g. $ZnSO_4$, $Zn(NO_3)_2$, $ZnCl_2$, $ZnBr_2$, ZnI_2 , followed similar procedures.

2.3 Characterization

XRD patterns were recorded on a diffractometer (AXS, Brucker, Germany) with Cu target (40 kV, 40 mA, λ=1.54059 Å) from 3^{o} to 55^{o} at a scan rate of 2^{o}/min with a step size of 0.02^{o}. The surface morphologies and elemental compositions of products were examined by SEM (SU-8020, Hitachi, Japan) coupled with Energy-dispersive X-ray spectroscopy (EDX) (INCA-X, Oxford, Japan) operated at an acceleration voltage of 1-15 kV in a high vacuum mode. Samples were mounted using a conductive carbon double-sided sticky tape. A thin (ca. 10 nm) coating of gold was sputtered onto the samples to reduce the effects of charging. The diameters of more than 200 particles in the SEM images were measured to determine the average particle size (d) and coefficient of variation (R^2) defined by Gaussian fitting equation. The nitrogen adsorption isotherms were measured at liquid nitrogen temperature (77 K) using a gas adsorption analyzer (ASAP2020HD88; Micromeritics, USA), the sample was degassed at 150 ^{o}C for 3 h under vacuum prior to measure. The surface

area was then calculated using the Brunauer-Emmett-Teller (BET) method based on adsorption data. pH values of solution were measured by a pH meter (Orion 3Star, Thermo, USA). The functional groups of products were identified by Fourier transform infrared spectroscopy (FT-IR) (Tenson 27; Bruker, Germany) in transmission mode.

3. Results and discussion

3.1 Effect of different zinc source

Fig. 1.

Fig. 1 shows the SEM images and XRD patterns of the ZIF-8 synthesized using different zinc precursors at variable Hmim/Zn ratios. It can be seen that variation of zinc salts is of a crucial factor in manipulating the morphology and crystalline phase of the resulting products. For example, when using $Zn(OAc)_2$ as zinc precursor, the morphology of synthesized particles exhibited truncated rhombic dodecahedron, with an exception of the product from the Hmim/Zn molar ratio of 10 which has a multilayered 2D structure (Fig. 1a). When $ZnSO_4$ was used, the particles prepared at the Hmim/Zn molar ratio of 70 showed bumpy surfaces but some truncated edges could be observed. Interestingly, like $Zn(OAc)_2$, the typical ZIF-8 particles with rhombic dodecahedron shape were obtained from $ZnSO_4$ in water at the molar ratios of 20 and 35 as well. The XRD patterns of the products are inserted in Fig. 1. The prominent reflections at $2\theta = 7.4^o$, 12.7^o and 18.0^o (marked with white squares) for the resulting products prepared at molar ratio of Hmim/Zn ranging from 20 to 70, were

observed clearly, which are in good agreement with simulated patterns of ZIF-8 single crystal with typical SOD structure.[12] However, using $Zn(OAc)_2$ at the Hmim/Zn molar ratio of 10, the peaks of *dia*(Zn) were disappeared, and the XRD results with unknown peaks (marked with orange squares) were observed (Fig. 1a, b inserted). Moreover, the products derived from $ZnSO_4$ are a dense *dia*(Zn) impurity with poorly resolved shapes (Fig. 1b). We hypothesize that the unexplored product could be immature ZIF-8 particles with some by-products such as $Zn(OH)_2$ or hydrous $Zn(OAc)_2$ compounds (see explanation in section 3.2).

In contrast, the molar ratios of Hmim/Zn $\geq$ 35 were required to generate pure ZIF-8 phase as shown in the XRD patterns of the products when using other zinc salts including $Zn(NO_3)_2$, $ZnCl_2$, $ZnBr_2$ and ZnI_2. At the Hmim/Zn molar ratios of 10, it seems that all resulting products exhibited a 2D leaf-layered structure regardless of zinc variations. This result is consistent with Yao et al. study, who demonstrated that 2D layered phase is an incubation form of ZIF-8 growth in water.[26] Meanwhile, various indeterminate morphologies were then observed at the Hmim/Zn molar ratio of 20 from different zinc precursors. The resulting samples prepared with $Zn(NO_3)_2$ displayed petal shapes while others showed rough spheroids (Fig. 1c, d, e, f). It is worth noting that almost all ZIF-8 particles prepared from zinc salts excepting $Zn(OAc)_2$ and $ZnSO_4$ in the water-based system were rather spherical surfaces instead of rhombic shapes at the Hmim/Zn = 35 and 70 although their XRD patterns both exhibited typical ZIF-8 crystalline phase. Last, it is worth mentioning that aqueous

room temperature synthetic strategy is highly efficient, as the yields of as-synthesized products were all over 90% based on zinc.

Fig. 2.

Furthermore, the size statistics of ZIF-8 particles prepared from different zinc salts were measured. As shown in Fig. 2, the sizes of the resulting particles decreased with an increase of the amount of Hmim. For example, the average size of particles prepared from $ZnSO_4$ decreases to 231 nm from 1.64 μm as Hmim/Zn ratio increases to 70 from 35. ZIF-8 particles prepared from $Zn(OAc)_2$ have a narrow size distribution with average particle size of around 746 nm at the Hmim/Zn = 70. The sizes of particles using $ZnCl_2$ and $Zn(NO_3)_2$ as zinc source are also smaller. The ZIF-8 synthesized using $ZnBr_2$ at the Hmim/Zn molar ratio of 70 has the narrowest size distribution with the mean size of only 26.4 nm. This result indicates that the crystal size of ZIF-8 depends on both Hmim concentration and zinc source.

In order to gain a better insight into ZIF-8 formation in water, $Zn(OAc)_2$ was used as an representative zinc source in the following experiments to investigate the effect of other synthesis condition.

3.2 Characterization of synthesized products at different Hmim/Zn ratios

Fig. 3.

N_2 sorption properties of the ZIFs obtained from variable Hmim/Zn molar ratios were measured (Fig. 3). The products prepared at the Hmim/Zn molar ratios ranging from 20 to 70 were found to exclusively exhibit typical type-I adsorption isotherms

with micropore domination. The BET specific surface area and total pore volume of the sample obtained from the Hmim/Zn molar ratio of 70 are 1126 m^2/g and 0.57 cm^3/g, respectively. This value is relatively close to the reported from literatures. It is worth noting that the BET surface area of particles prepared decreases with the decrease of the Hmim/Zn molar ratio. This could be attributed to the larger particle size distributions at low Hmim/Zn molar ratio. In addition, the adsorbed N_2 amount near P/P_0 = 1 increased, indicating highly interparticle porosity between ZIF-8 particles, which is also confirmed by SEM results. However, at the Hmim/Zn molar ratio of 10, the resultant sample exhibits limited amount of N_2 adsorption with the lowest BET value of 31.9 m^2/g and the pore volume was 0.15 cm^3/g, which reveals that the 2D material with weak porosity possesses distinctive textural property.

Fig. 4.

The chemical functional groups of products that prepared at various Hmim/Zn molar ratios were examined by FT-IR spectroscopy. As shown in Fig. 4d, at the Hmim/Zn molar ratio of 70, the bands at 687 and 754 cm^{-1} in the fingerprint region are associated with out-of-plane bending of the Hmim ring, whereas peaks in the region of between 900 and 1350 cm^{-1} arise from the in-plane bending.[27] The peaks at 1678 and 1581 cm^{-1} are attributed to the bending and stretching N-H vibration of the Hmim, respectively.[21] The intense and convoluted bands at 1425 cm^{-1} are associated with the entire ring stretching, whereas two weak peaks at 2930 and 3124 cm^{-1} can be assigned as the aliphatic and aromatic C-H stretching of the Hmim, respectively (Fig. 4d).[28] Meanwhile, the representative Zn-N stretching band

was also observed at the position of around 418 cm^{-1}.[29] Noticeably, consistent results are also obtained from products that synthesized at the Hmim/Zn of 20 and 35 (Fig. 4b, c). These FT-IR results are consistent with pure ZIF-8 that previously reported in the literature,[30] confirming again that the products prepared from $Zn(OAc)_2$ in water are pure ZIF-8 crystals. Interestingly, for the product with 2D structure that prepared at the lowest Hmim/Zn molar ratio, the FT-IR spectrum shows a close similarity with others, indicating that the 2D multilayered material is made up of the same building units as ZIF-8 crystals despite of different topotactic phases (Fig. 4a). But it should be noted that the absorbance bands at 427 cm^{-1} induces a slight blue shift of Zn-N stretching frequency (+8 cm^{-1}), signifying that Zn-N coordination model may be different from pure ZIF-8 at low Hmim concentration.

Fig. 5

SEM/EDX analysis was conducted to characterize the elementary data, which further support the chemical composition of the resultant 2D product generated at the Hmim/Zn molar ratio of 10 (Fig. 5). According to the results of EDX, the Zn to N ratio was calculated to be 1:2.2. This value is much higher than the simulated ZIF-8 elemental ratio of 1:4, where the stoichiometric molar ratio of Zn and Hmim in ZIF-8 is 1:2. This suggests that other zinc-based clusters growth may be involved at low Hmim/Zn molar ratio that is different from conventional $Zn(mim)_2$ cluster. However, this, together with FT-IR results demonstrated that the new 2D structure consists of Zn and Hmim, and we speculate that the layered structure could be an

intermediate form of ZIF-8 crystals. The consequence may result from decreasing the amount of deprotonated linkers at a low Hmim concentration, which limits the rate of phase transformation. Similar study has been reported.[26, 31]

3.3 Effect of water content

Fig. 6.

Fig. 6 shows effect of the water amount in the synthesis of ZIF-8 crystals on XRD patterns at the constant Hmim/Zn molar ratio of 10. When the water content decreased from the Zn/Hmim/H_2O molar ratio of 1/10/2476 to 1/10/1238, the products exhibit the same diffraction peaks with unidentified XRD phases, which can be indexed to some by-products. However, with decreasing water amount to Zn/Hmim/H_2O molar ratio of 1/10/805, the intensity of reflection peaks of the by-products decreased and the notable peak of *dia*(Zn) for ZIF-8, corresponding to the {011} plane, appeares. Moreover, the intensity of {011} peak increases as the amount of water decreases further (Fig. 6). Similar result was also found by the previous report.[25] On the other hand, we noticed that high concentration of precursor solution triggered a rapid coordination reaction. The solution prepared at the Zn/Hmim/H_2O molar ratio of 1/10/310 turns completely cloudy within 90 s, although precipitates appeared in all solutions after aging 24 h (Fig. 6 inserted). It is worth noting that we found zinc concentration has less effect on the color change in solution (data not shown). This observation indicates that the high Hmim concentration may significantly accelerate the nucleation process of ZIF-8 crystals.

Fig. 7.

Shape variations of the resulting products prepared in different water content were observed by SEM, as shown in Fig. 7. The morphology of the products shifts from a multilayered structure to typical ZIF-8 crystals with reducing the water amount. For example, with the Zn/Hmim/H_2O molar ratio of 1/10/310, uniform truncated rhombic dodecahedral particles were obtained with the typical ZIF-8 topology (Fig. 7a). However, samples synthesized at low concentration of solution remained a similar shape with 2D multilayered structure (consistent with XRD results) in Fig. 7d, e and f. Furthermore, the particles prepared at the Zn/Hmim/H_2O molar ratio of 1/10/619 and 1/10/805 have rough and deformed morphology with many defects around the surfaces, indicating a low crystallization level (Fig. 7b, c).

3.4 Time-dependent structural evolution of ZIF-8 crystals

Fig. 8.

Fig. 8 shows the pH variation as function of reaction time. It can be observed that the initial pH of the precursor solutions (Hmim solution) at different Hmim/Zn molar ratios are all around 11.0. When Zn-based solution is added, the solution pH decreases drastically to 10.0, 9.7, 9.3 and 9.6 within 5 s for the mixtures at the Hmim/Zn molar ratio of 70, 35, 20 and 10, respectively. After that, the pH values remain constant, with an exception of the solution at the minimal Hmim/Zn = 10. The rapid pH change indicates that the nucleation stage for ZIF-8 crystals growth in water is very fast. It is further proven that milky colloidal mixtures are formed after a few

minutes (Fig. 9).

Fig. 9.

Fig. 10

Afterwards, complementary SEM investigation was carried out for the sample prepared at the Zn/Hmim/H_2O molar ratio of 1/35/1238 to confirm formation and growth of the ZIF-8 crystals as a function of synthesis time (Fig. 10). As the yield is extremely low and the size is remarkably small in the first 5 min (Fig. 9), we were not able to record the SEM images. At 5 min, the spherical particles with bumpy surfaces are observed. With increasing the time to 20 and 60 min, the crystals begin to display heterogeneous hexagonal facet, this period is the metastable phase for ZIF-8 growth. At 4 h, the surface of ZIF-8 crystals became smooth and homogeneous with few defects (enclosed by 8 {011} and 6 {001} facets). As time progresses further to 8 h, many tiny ZIF-8 crystallites are formed, while the amount became insignificant at 16 h, this phenomenon could be explained by Ostwald ripening mechanism.[32] Finally, the rhombic dodecahedron shape with 12 {011} surfaces, well known as typical ZIF-8 morphology, are observed at 16 h and this equilibrium shape is maintained even after 3 d. It is known that the morphology of crystals is mainly determined by the surface energy of the crystal facets and rhombic dodecahedral crystallites with exposing 12 {011} faces have the lowest surface energy and the most stable structure, which is the equilibrium form of ZIF-8 crystal.[33]

Fig. 11.

Fig. 11 compares the change of XRD of the synthesized ZIF-8 with the synthesis time. Clearly, at the very initial period within only 5 minutes from $Zn(OAc)_2$, the typical XRD patterns of ZIF-8 can be readily obtained despite relatively weak peak of *dia*(Zn) for ZIF-8 at $2\theta = 7^o$. However, the prominent peak, corresponding to the {011} plane of SOD-type ZIF-8 crystal, increases with reaction time. Furthermore, we quantified the {011} peak area under the Gaussian fitting curve after baseline correction, to determine the relative crystallinity level of ZIF-8 particles at different phases (Table 1) according to Venna's method.[34] The relative crystallinity of ZIF-8 particles was in a low degree (about 15-20%), but a rapid increase was shown at 8 h. Next, the value increased to 97% at 16 h and stayed practically unchanged until reaching a maximum of 100% at 3 d.

Table 1

3.5 ZIF-8 growth mechanism in water

Fig. 12.

Based on the above results, we put forward a synthesis mechanism for ZIF-8 crystals growth in the water-based system in Fig. 12, which includes hydrolysis, coordination and deprotonation. In the context of ZIF-8 formation, it is well known that the deprotonating Hmim (mim^- ions) in the solution is required to bridge the solvated zinc ions to form building units. However, the deprotonation of Hmim is not able to occur in water because of its high pK_a value (pK_a [Hmim] = 14.2).[19] Instead, the ligand Hmim mostly runs hydrolysis reaction in aqueous solution. Thus Hmim

only exhibits two forms of Hmim and H_2mim^+ in water and this is also the main reason why Hmim solution is basic. After this stage, zinc ions are most likely to link the Hmim via coordination process to form $Zn(Hmim)_n^{2+}$ ($1 \leq n \leq 4$) units. This period is the time when the pH start to drop dramatically because the equilibrium equation of Hmim during hydrolysis progress toward the left-hand side along with the rapid consumption of Hmim during the coordination process. An excess of Hmim can be the moderate deprotonation agent to enable $Zn(Hmim)_n^{2+}$ to lose protons cation, resulting in forming ZIF-8 crystals in water eventually. This is because that Hmim owns a higher the deprotonation constant than the intermediate product of $Zn(Hmim)_n^{2+}$ (pKa = 10.3).[19] Meanwhile, this is the crucial point that aqueous synthesis requires excessive Hmim ligands to obtain phase-pure ZIF-8.

Scheme 1

Therefore, a five-step process in the morphology transformation of ZIF-8 growth in water is deduced (Scheme 1). The first step of the process is considered to be nucleation phase, where zinc ions mixed with Hmim in water and prepared to form tiny crystal nucleus. During the nucleation process, a rapid nucleation rate will hinder the growth of ZIF-8 significantly.[35] Thus nucleation rate plays a key role in crystal formation, which influenced by precursor concentration. From the previous report, OAc^- is expected to be relatively strong bond energy to zinc to form a Zn-acetate complex, which leads to a slow nucleation rate and promotes the formation of ZIF-8.[36] In contrast, $ZnSO_4$ has no capability of slowing down the nucleation rate because we observed that addition of $ZnSO_4$ solution caused the immediate cloudy

precipitation. Moreover, SO_4^{2-} cannot effectively deprotonate $Zn(Hmim)_n^{2+}$ species ($pK_a[H_2SO_4] < 10.3$). Therefore, from the Hofmeister effect point of view, we assume that SO_4^{2-} anions may change the hydrolysis rates of the precursors of zinc and Hmim, affecting the surface self-assembly and morphologies of the final products, because SO_4^{2-} owns the strongest Hofmeister effect among other anions of the listed zinc salts.[37] Very recently, Chen et al. reported the similar results in the aqueous ammonia solution.[38]

The second step is the growth of the nuclei up to 2D layer-structured products with a larger size. The 2D flake products are actually the transient crystalline phase of ZIF-8, which caused by the insufficient protonated Hmim ligands in water. This point has also been well investigated by Yao et al., who demonstrated that the 2D layers were stacked each other via the hydrogen bond instead of free mim^-.[26] Following this, the extra amount of Hmim ligands in water results in a rapid increase in the number of the intermediate products, and starts to random attachment between 2D layers units, which is termed as layer-by-layer growth in the crystal growth theory.[39, 40] Many layered crystals are randomly aggregated from this stage onwards, resulting in multilayered structure. Afterwards, the excess of Hmim undergoes deprotonation of Zn-Hmim complexes to form ZIF-8 crystals, stacked layers break down to smaller crystals. In this stage, the Zn-Hmim bonds are broken and reform new Zn-mim-Zn coordinate bonds, which are composing of developed ZIF-8 structure. The final step is classified as the stationary phase, the metastable ZIF-8 nanocrystals in last stage starts to grow larger *via* the Ostwald ripening process. On the basis of the heterogeneous

growth mechanism, this variation occurs under specific synthesis conditions where provides decelerated crystallization speed or strong Hofmeister effect for ZIF-8 structural transformation.[41] As a result, the growing crystals undergo the equilibrium state toward a minimum free energy with a rhomboid shape, which is homogeneous pure ZIF-8 crystal.[33, 42]

4. Conclusions

In conclusion, this study demonstrated that high-quality ZIF-8 particles can be produced in water at room temperature based on the use of the proper zinc salt as metal source. The use of $Zn(OAc)_2$ or $ZnSO_4$ is found to generate high crystalline ZIF-8 with large size particles and have favorable effect in reducing the consumption of Hmim. During the synthesis process, we found that particle sizes and shapes of resulting ZIF-8 materials can be readily controlled by the amount of Hmim. Moreover, long synthesis time promotes the complete crystallization of ZIF-8. Furthermore, we demonstrate that the kinetics of transformation of ZIF-8 in water involves 3 key reactions including hydrolysis, coordination and deprotonation. Finally, we believe this green and facile-synthesis strategy can be widely-applicable in large-scale production of ZIF-8.

Acknowledgements

This work was partially supported by the key project of the National “863” High-tech R&D Program of China (2012AA062604). The authors would like to acknowledge the Joint Research Fund for Overseas Chinese Scholars and Scholars in Hong Kong

and Macao (51328803) awarded by the National Natural Science Foundation of China.

Notes and references

[1] H.-C. Zhou, S. Kitagawa, *Chem. Soc. Rev.*, 2014, **43**, 5415-5418.

[2] G. Xu, T. Yamada, K. Otsubo, *J. Am. Chem. Soc.*, 2012, **134**, 16524-16527.

[3] B. Chen, Z. Yang, Y. Zhu, Y. Xia, *J. Mater. Chem. A.*, 2014, **2**, 16811-16831.

[4] J-R Li, J Sculley and H-C Zhou, *Chem. Rev.*, 2012, **112**, 869-932.

[5] J. Liu, L. Chen, H. Cui, J. Zhang, L. Zhang, C-Y. Su, *Chem. Soc. Rev.*, 2014, **43**, 6011-6061.

[6] T. Zhang, W. Lin, *Chem. Soc. Rev.*, 2014, **43**, 5982-5993.

[7] Z. Hu, B.J. Deibert, J. Li, *Chem. Soc. Rev.*, 2014, **43**, 5815-5840.

[8] L.E. Kreno, K. Leong, O.K. Farha, M. Allendorf, R.P.V. Duyne, J.T. Hupp, *Chem. Rev.*, 2011, **112**, 1105-1125.

[9] P. Horcajada, R. Gref, T. Baati, P.K. Allan, G. Maurin, P. Couvreur, G. Férey, R.E. Morris, C. Serre, *Chem. Rev.*, 2012, **112**, 1232-1268.

[10] C.-C. Wang, J.-R. Li, X.-L. Lv, Y.-Q. Zhang, G. Guo, *Energy. Environ. Sci.*, 2014, **7**, 2831-2867.

[11] Z. Hasan, S.H. Jhung, *J. Hazard. Mater.*, 2015, **283**, 329-339.

[12] K.S. Park, Z. Ni, A.P. Côté, J.Y. Choi, R. Huang, F.J. Uribe-Romo, H.K. Chae, M. O'Keeffe, O.M. Yaghi, *Porc. Nat. Acad. Sci. U.S.A.*, 2006, **103**, 10186-10191.

[13] L.Z.a.Y.H. Hu, *J. Phys. Chem. C.*, 2011, **115**, 7967-7971.

[14] Y-R. Lee, J Kim, W-S. Ahn, *Korean J. Chem. Eng.*, 2013, **30**, 1667-1680.

[15] X.-C. Huang, Y.-Y. Lin, J.-P. Zhang, X.-M. Chen, *Angew. Chem. Int. Ed.*, 2006, **45**, 1557-1559.

[16] J Cravillon, S Munzer, S-J Lohmeier, A Feldhoff, K Huber, M Wiebcke, *Chem. Mater.*, 2009, **21**, 1410-1412.

[17] A.F. Gross, E. Sherman, J.J. Vajo, *Dalton Trans.*, 2012, **41**, 5458-5460.

[18] M.C. Mccarthy, V. Varela-guerrero, G.V. Barnett, H.-k. Jeong, *Langmuir.*, 2010, **26**, 14636-14641.

[19] J Cravillon, R. Nayuk, S. Springer, A. Feldhoff, K. Huber, M. Wiebcke, *Chem. Mater.*, 2011, **23**, 2130-2141.

[20] Y.-Q. Tian, Y.-M. Zhao, Z.-X. Chen, G.-N. Zhang, *Chem. Eur. J.*, 2007, **13**, 4146-4154.

[21] M. He, J. Yao, Q. Liu, K. Wang, F. Chen, H. Wang, *Microporous Mesoporous Mater.*, 2014, **184**, 55-60.

[22] Y. Pan, D. Heryadi, F. Zhou, L. Zhao, G. Lestari, H. Su, Z. Lai, *CrystEngComm.*, 2011, **13**, 6937-6940.

[23] S. K. Nune, P. K. Thallapally, A. Dohnalkova, C. Wang, J. Liu, G. J. Exarhos, *Chem. Commun.*, 2010, **46**, 4878-4880.

[24] Y. Pan, Y. Liu, G. Zeng, L. Zhao, Z. Lai, *Chem. Commun.*, 2011, **47**, 2071-2073.

[25] K Kida, M Okita, K Fujita, S Tanaka, Y Miyake, *CrystEngComm.*, 2013, **15**, 1794-1801.

[26] R. Chen, J. Yao, Q. Gu, S. Smeets, C. Baerlocher, H. Gu, D. Zhu, W. Morris, O.M. Yaghi, H. Wang, *Chem. Commun.*, 2013, **49**, 9500-9502.

[27] M. Jian, B. Liu, G. Zhang, R. Liu, X. Zhang, *Colloids Surf. A-Physicochem. Eng. Asp.*, 2015, **465**, 67-76.

[28] Z.-X. Low, J. Yao, Q. Liu, M. He, Z. Wang, A.K. Suresh, J. Bellare, H. Wang, *Cryst. Growth Des.*, 2014, **14**, 6589-6598.

[29] Y. Hu, H. Kazemian, S. Rohani, Y. Huang, Y. Song, *Chem. Commun.*, 2011, **47**, 12694-12696.

[30] Y. Hu, Z. Liu, J. Xu, Y. Huang, Y. Song, *J. Am. Chem. Soc.*, 2013, **135**, 9287-9290.

[31] P.-Z. Li, Y. Maeda, Q. Xu, *Chem. Commun.*, 2011, **47**, 8436-8438.

[32] S.R. Challa, A.T. Delariva, T.W. Hansen, S. Helveg, J. Sehested, P.L. Hansen, F. Garzon, A.K. Datye, *J. Am. Chem. Soc.*, 2011, **133**, 20672-20675.

[33] Q. Liu, J.-M. Yang, L.-N. Jin, W.-Y. Sun, *Chem. Eur. J.*, 2014, **20**, 14783-14789.

[34] S.R. Venna, J.B. Jasinski, M.A. Carreon, *J. Am. Chem. Soc.*, 2010, **132**, 18030-18033.

[35] J. Cravillon, C.a. Schröder, R. Nayuk, J. Gummel, K. Huber, M. Wiebcke, *Angew. Chem. Int. Ed.*, 2011, **123**, 8067-8071.

[36] S. Tanaka, T. Shimada, K. Fujita, Y. Miyake, K. Kida, K. Yogo, J.F.M. Denayer, M. Sugita, T. Takewaki, *J. Membrane. Sci.*, 2014, **472**, 29-38.

[37] E. Leontidis, *Curr. Opin. Colloid. In.*, 2002, **7**, 81-91.

[38] B. Chen, F. Bai, Y. Xia, *RSC Adv.*, 2014, **4**, 47421-47428.

[39] W.K. Burton, N Cabrera, F.C. Frank, *Phil. Trans. R. Soc. A.*, 1951, **243**, 299-358.

[40] M. Hu, S. Ishihara, Y. Yamauchi, *Angew. Chem. Int. Ed.*, 2013, **52**, 1235-1239.

[41] N. T. K. Thanh, N. Maclean, S. Mahiddine, *Chem. Rev.*, 2014, **114**, 7610-7630.

[42] Y. Sakata, S. Furukawa, M. Kondo, K. Hirai, N. Horike, Y. Takashima, H. Uehara, N. Louvain, M. Meilikhov, T. Tsuruoka, S. Isoda, W. Kosaka, O. Sakata, S. Kitagawa, *Science*, 2013, **339**, 193-196.

List of Figure Captions:

Fig. 1. SEM images and PXRD patterns (inserted) of the products obtained from different Hmim/Zn ratios and starting from (a) $Zn(OAc)_2$, (b) $ZnSO_4$, (c) $Zn(NO_3)_2$, (d)$ZnCl_2$, (e) $ZnBr_2$, (f) ZnI_2.

Fig. 2. Comparison of average size of ZIF-8 particles obtained from 6 different zinc precursors at the Hmim/Zn ratio of 70 and 35.

Fig. 3. Nitrogen isotherms of the products prepared from $Zn(OAc)_2$ at Hmim/Zn molar ratios of (a) 70, (b) 35, (c) 20 and (d) 10. Solid and hollow data correspond to the adsorption and desorption branches, respectively.

Fig. 4. FT-IR spectra of synthesized samples prepared from $Zn(OAc)_2$ at Hmim/Zn molar ratios of (a) 10, (b) 20, (c) 35 and (d) 70.

Fig. 5. SEM/EDX analysis for the sample obtained at the Hmim/Zn ratio of 10 using $Zn(OAc)_2$.

Fig. 6. PXRD patterns of synthesized samples in different water amount at the constant Hmim/Zn molar ratio of 10.

Fig. 7. SEM images of the products prepared from $Zn(OAc)_2$ with different water amounts: (a) 310, (b) 619, (c) 805, (d) 1238, (e) 1610 and (f) 2476 at the constant Hmim/Zn molar ratio of 10. Scale bars: 1 μm.

Fig. 8. Change of solution pH as a function of synthesis time at different Hmim/Zn molar ratios.

Fig. 9. Photographs of synthesis solution at Zn/Hmim/H_2O molar ratio of 1/35/1238 as a function of time.

Fig. 10. Shape evolution of synthesized ZIF-8 obtained from $Zn(OAc)_2$ as a function of reaction time in water with Zn/Hmim/H_2O molar ratio of 1/35/1238.

Fig. 11. PXRD patterns of the products prepared at the Hmim/Zn molar ratio of 35 as a function of synthesis time.

Fig. 12. Proposed mechanism for the formation of ZIF-8 crystals in water.

Scheme 1. Proposed formation pathway of the growth of ZIF-8 crystals in water [a]

Table 1. ZIF-8 relative crystallinity as a function of synthesis time.

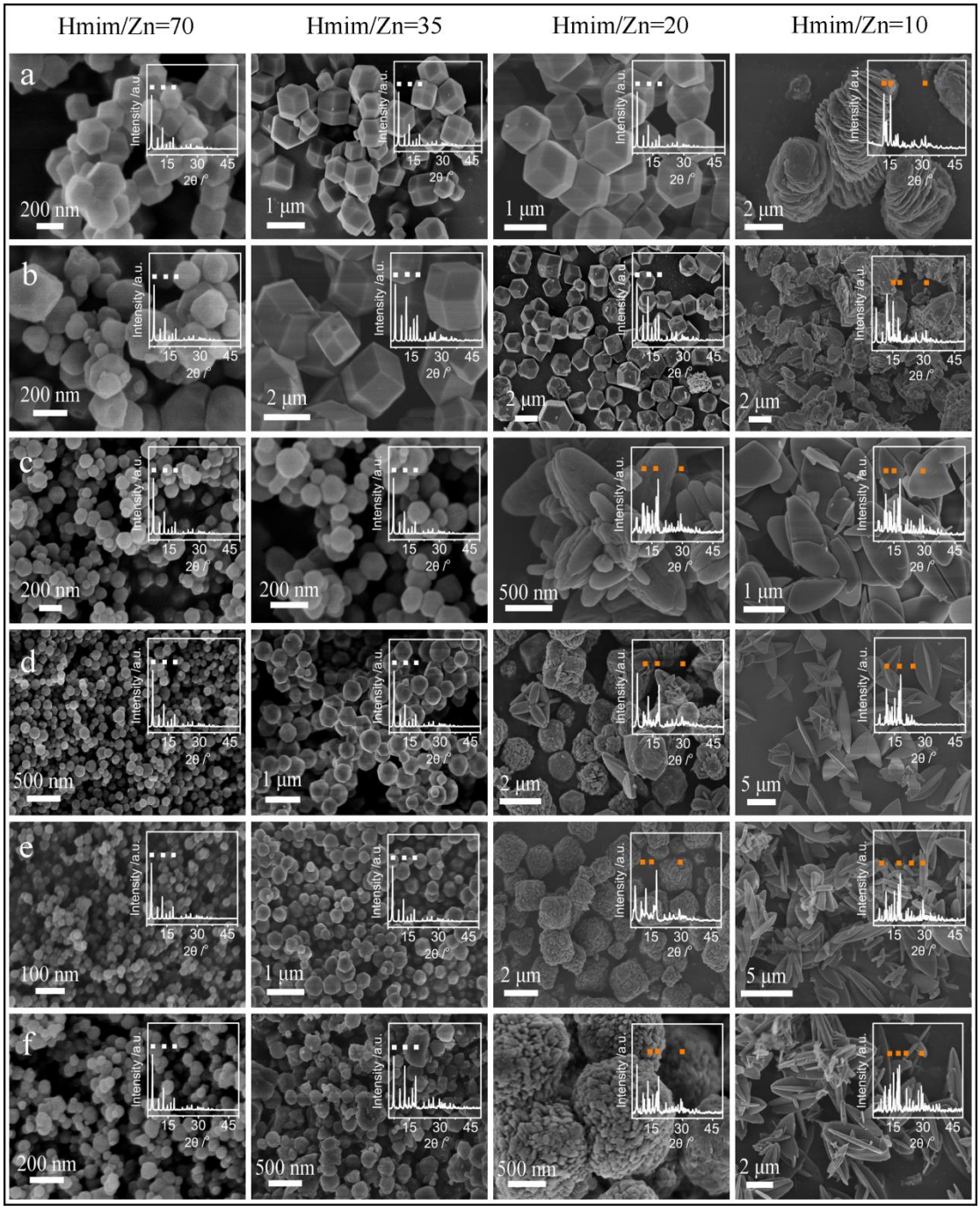

Fig. 1. SEM images and PXRD patterns (inserted) of the products obtained from different Hmim/Zn ratios and starting from (a) $Zn(OAc)_2$, (b) $ZnSO_4$, (c) $Zn(NO_3)_2$, (d)$ZnCl_2$, (e) $ZnBr_2$, (f) ZnI_2.

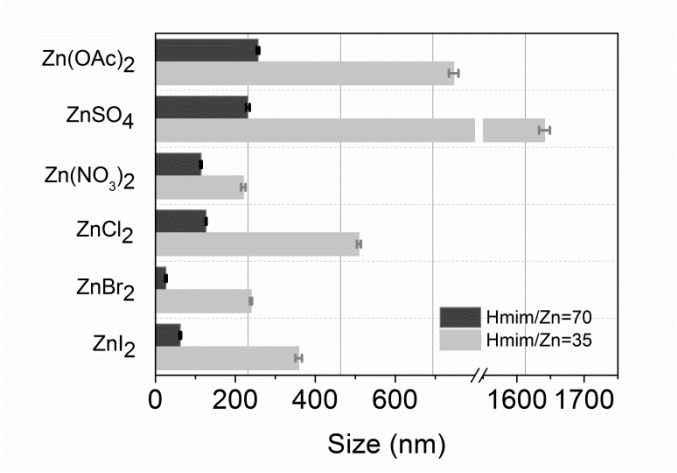

Fig. 2. Comparison of average size of ZIF-8 particles obtained from 6 different zinc precursors at the Hmim/Zn ratio of 70 and 35.

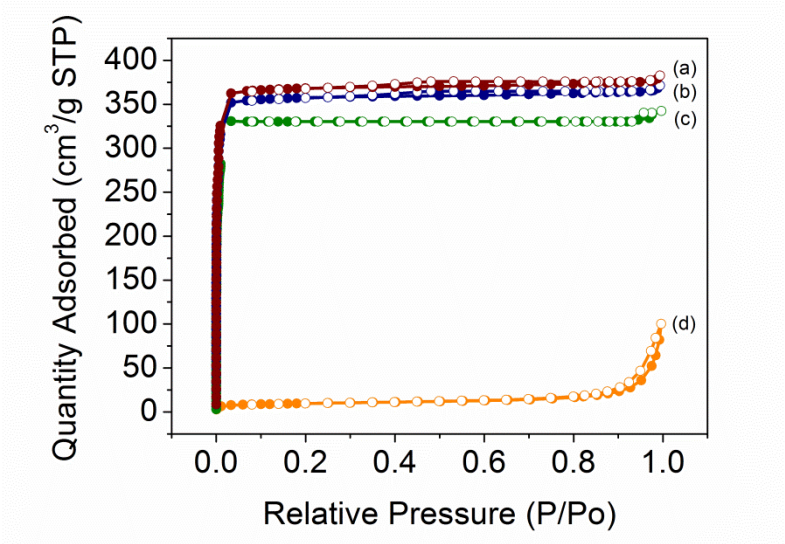

Fig. 3. Nitrogen isotherms of the products prepared from $Zn(OAc)_2$ at Hmim/Zn molar ratios of (a) 70, (b) 35, (c) 20 and (d) 10. Solid and hollow data correspond to the adsorption and desorption branches, respectively.

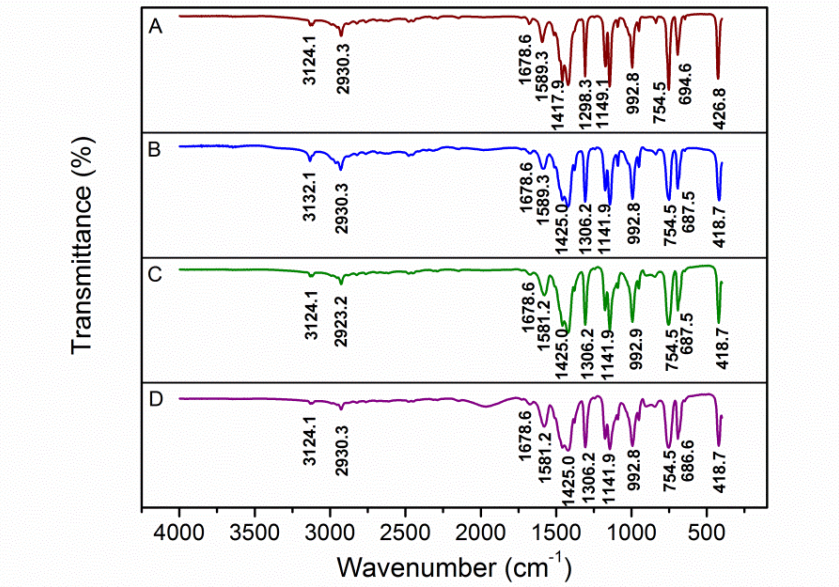

Fig. 4. FT-IR spectra of synthesized samples prepared from $Zn(OAc)_2$ at Hmim/Zn molar ratios of (a) 10, (b) 20, (c) 35 and (d) 70.

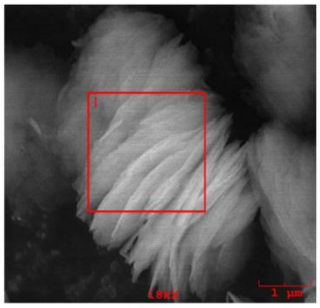

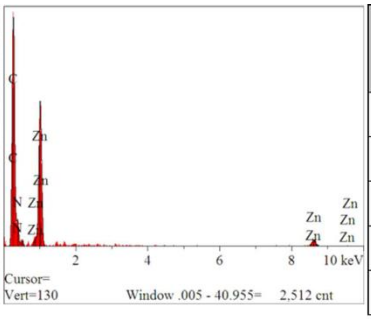

Elt.	Intensity c/s	Atomic %	Conc. wt. %
C	53.66	61.063	50.771
N	6.55	31.489	30.531
O	1.90	4.390	4.862
Zn	4.04	3.058	13.836
Total		100.000	100.000

Fig. 5. SEM/EDX analysis for the sample obtained at the Hmim/Zn ratio of 10 using $Zn(OAc)_2$.

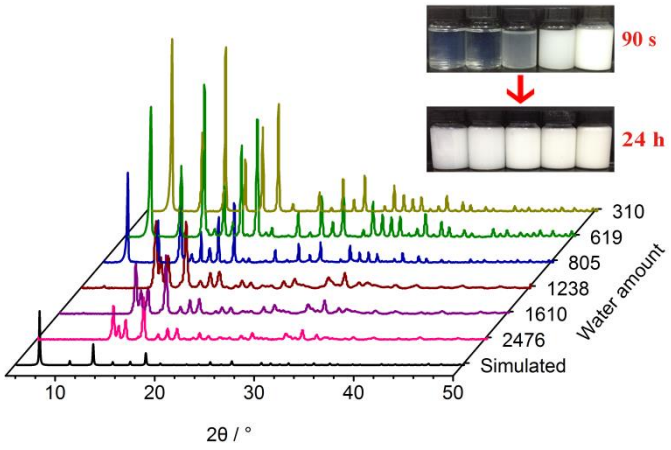

Fig. 6. PXRD patterns of synthesized samples in different water amount at the constant Hmim/Zn molar ratio of 10.

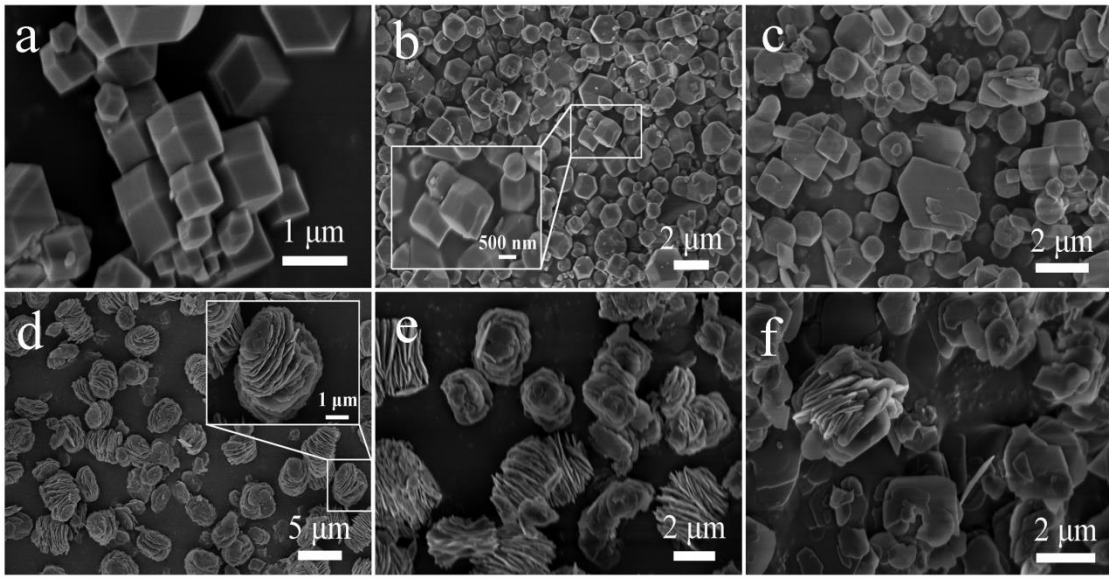

Fig. 7. SEM images of the products prepared from $Zn(OAc)_2$ with different water amounts: (a) 310, (b) 619, (c) 805, (d) 1238, (e) 1610 and (f) 2476 at the constant Hmim/Zn molar ratio of 10.

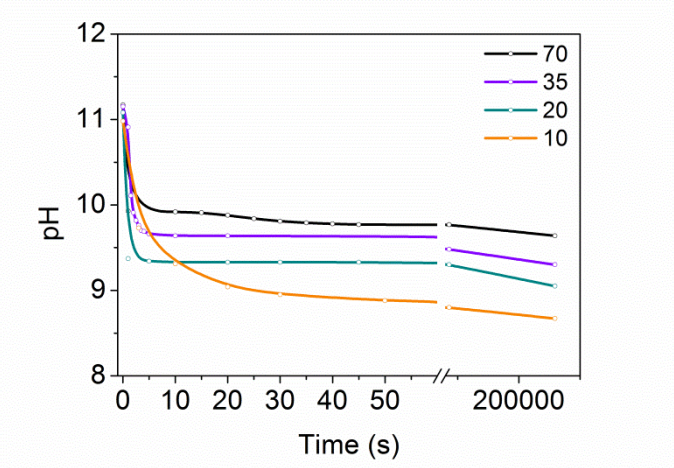

Fig. 8. Change of solution pH as a function of synthesis time at different Hmim/Zn molar ratios.

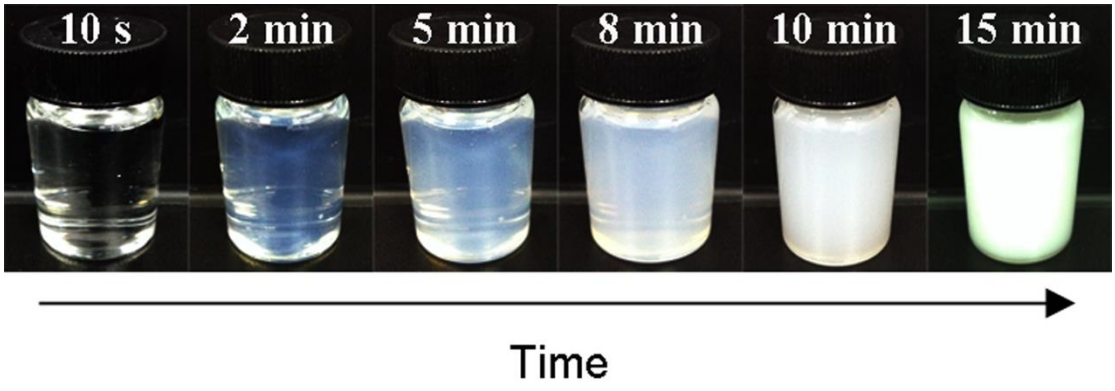

Fig. 9. Photographs of synthesis solution at Zn/Hmim/H_2O molar ratio of 1/35/1238 as a function of time.

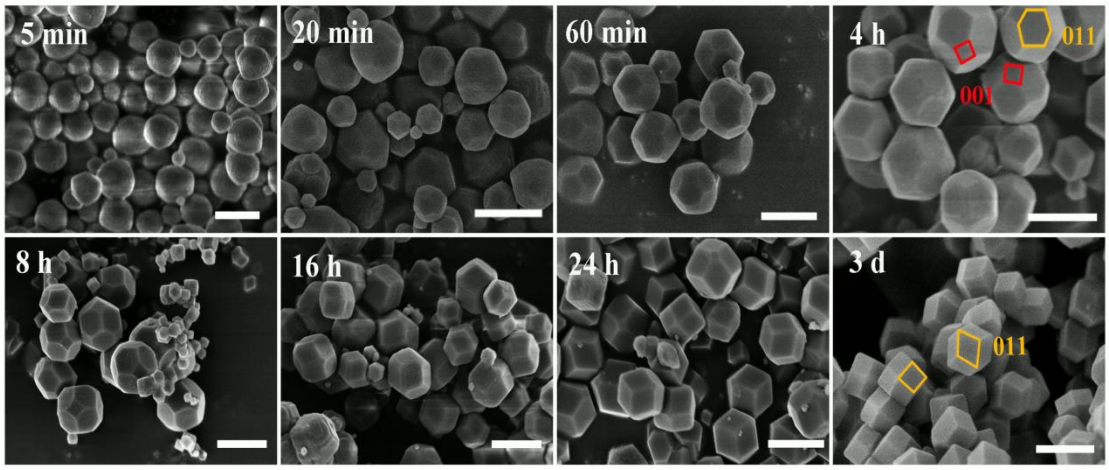

Fig. 10. Shape evolution of synthesized ZIF-8 obtained from $Zn(OAc)_2$ as a function of reaction time in water with Zn/Hmim/H_2O molar ratio of 1/35/1238. Scale bars: 1 μm.

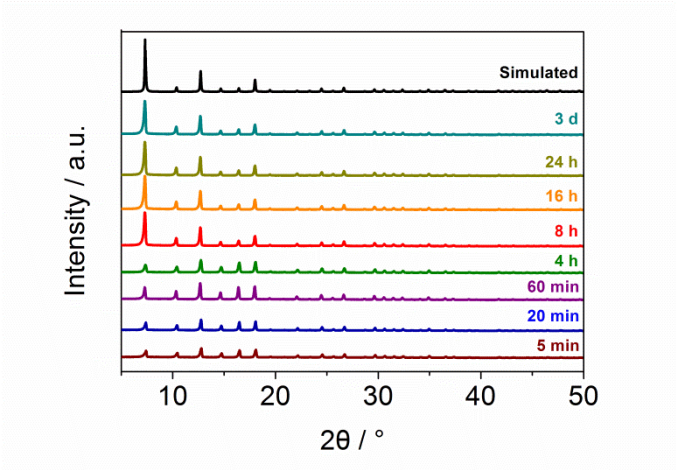

Fig. 11. PXRD patterns of the products prepared at the Hmim/Zn molar ratio of 35 as a function of synthesis time.

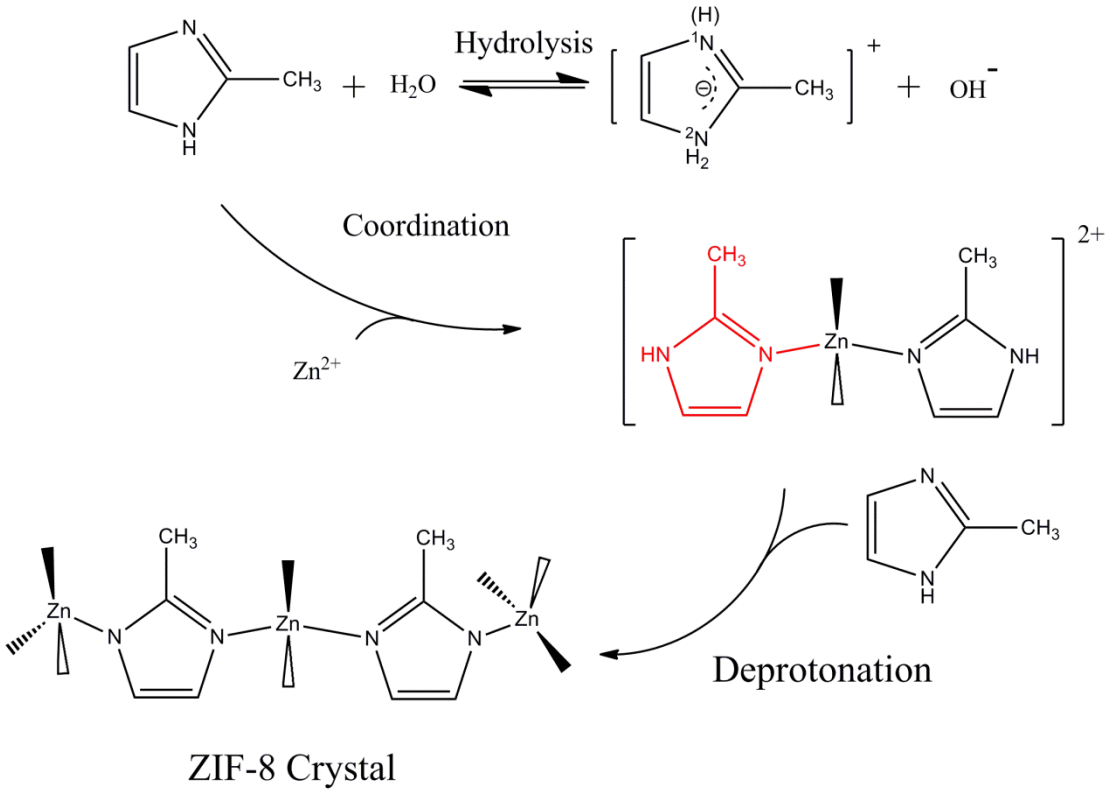

Fig. 12. Proposed mechanism for the formation of ZIF-8 crystals in water.

Scheme 1. Proposed formation pathway of the growth of ZIF-8 crystals in water [a]

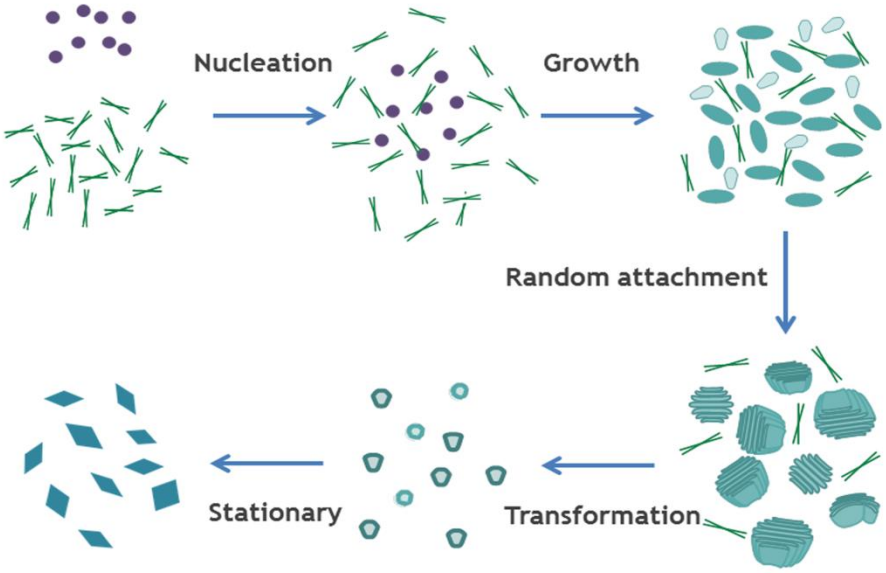

[a] The purple spheres and green rods represent zinc ion and free Hmim, respectively.

Table 1. ZIF-8 relative crystallinity as a function of synthesis time

Synthesis time	Area under the curve	% Crystallinity
5 min	1950	15.99
20 min	1895	15.54
60 min	2856	23.42
4 h	2405	19.72
8 h	9107	74.66
16 h	11935	97.85
24 h	11446	93.84
3 d	12197	100

* The ZIF-8 relative crystallinity was calculated with the following expression:

$$\% \text{ ZIF-8 relative crystallinity} = \frac{Area\ under\ the\ curve\ (011)\ plane\ at\ a\ time}{Area\ under\ the\ curve\ (011)\ plane\ at\ 3\ d}$$

The area under the curve was obtained from the value of the Gaussian fitting of the data.

Water-based synthesis of zeolitic imidazolate framework-8 with high morphology level at room temperature

Graphical Abstract:

Additives-free synthesis of ZIF-8 with perfect morphology in water at room temperature involves 3 key reactions and 5 evolutional steps.